タイトル Title	Selective dealkylation of alkyl polycyclic aromatic hydrocarbons towards innovative upgrading process of practical heavy oil
著者 Auther(s)	Nakano, Fumiya; Goma, Tomohide; Suganuma, Satoshi; Tsuji, Etsushi; Katada, Naonobu
掲載誌・巻号・ページ Citation	CATALYSIS SCIENCE & TECHNOLOGY , 11 (1) : 239 - 249
刊行日 Issue Date	2021-01-07
資源タイプ Resource Type	学術雑誌論文 / Journal Article
版区分 Resource Version	著者版 / Author
権利 Rights	(C) The Royal Society of Chemistry 2021
DOI	10.1039/d0cy01590c
URL	https://repository.lib.tottori-u.ac.jp/11579

Selective dealkylation of alkyl polycyclic aromatic hydrocarbons towards innovative upgrading process of practical heavy oil

Fumiya Nakano, Tomohide Goma, Satoshi Suganuma,* Etsushi Tsuji, Naonobu Katada

Center for Research on Green Sustainable Chemistry, Tottori University, 4-101 Koyama-cho Minami, Tottori 680-8552, Japan

Phone: +81-857-31-5256; Fax: +81-857-31-5684; E-mail: suganuma@tottori-u.ac.jp

Abstract

Dealkylation of alkyl polycyclic aromatic hydrocarbons (APAHs) in vacuum gas oil (VGO) was studied as a novel upgrading process alternative to conventional processes. A silica-monolayer loaded on alumina (SMA) with weak Brønsted acid sites and large pore size exhibited higher activity than amorphous silica-alumina and zeolites (USY and ZSM-5). SMA almost completely converted the APAHs into aromatics and alkanes, but a small amount of APAHs with methyl and ethyl groups (short-chain) were unreacted. Larger pore size of SMA was proposed to be enough for bulky APAHs to diffuse. The dealkylation by SMA formed large amounts of long-chain alkanes, which can be utilized as light oil and kerosene for fuel, lubricating oil, etc. The cracking of long-chain alkanes did not proceed, and thus scarcely formed lighter alkanes. SMA in the reaction adsorbed alkanes but did not form coking, and therefore exhibited continuous dealkylation activity. Additionally, it was revealed that the pore size of SMA slightly affected the composition of the formed alkanes.

24

1. Introduction

Petroleum refineries are generally developed for the production of transportation fuels, but perform minor but essential production of building blocks for petrochemicals, such as light alkenes (ethylene and propylene) and BTEX (benzene, toluene, ethylbenzene, and xylenes) [1-4]. The transportation fuels are produced by atmospheric distillation, while the atmospheric residue oil is processed by vacuum distillation. The vacuum gas oil (VGO) is converted into gasoline, light oil, and kerosene by fluid catalytic cracking (FCC), hydrocracking, or thermal cracking. However, the growing rate of demand in transportation fuel is declining due to improvement of fuel consumption of vehicles and control of carbon dioxide emission [5]. Yield of the petrochemicals is limited based on the operation conditions, which are designed to fit the demands of transportation fuel. Recently, an FCC process has been developed for increasing production of light alkenes, but yield of benzene derivatives cannot be increased by further reorganization of the process. On the other hand, the hydrocracking process consumes a large amount of hydrogen for hydrogenation of polycyclic aromatic hydrocarbons, which leads to a decrease of benzene derivative yields due to the severe hydrogenation condition. Benzene derivatives are applied as the chemicals and their intermediates of synthetic fibers, resins, detergents, and various organic ingredients. Among the benzene derivatives, the manufacture volumes of benzene and paraxylene are notably increasing. However, production of benzene derivatives is complicated for FCC and hydrocracking. Therefore, innovation of petroleum refineries for increasing flexibility in the production is strongly required, in order to cope with the change of situation.

We have studied an alternative process to FCC and hydrocracking [6-9], and an outline was given in a review [10]. The components in VGO are categorized into 3 main types: aliphatics (alkanes as main components), aromatics, and alkylaromatics. If the alkyl polycyclic aromatic hydrocarbons (APAHs) are completely dealkylated to alkanes and PAHs with no alkyl groups, the components can be facilely separated into 2 types by such methods as solvent extraction [11-13]. The dealkylation of an APAH via β-scission of a carbenium ion is catalyzed by Brønsted acid sites, like cracking of cumene (2-phenylpropane) [14,15], forming an aromatic hydrocarbon and a carbenium ion. Then, alkanes are formed from the carbenium ions through the presumed reaction pathways as follows: hydrogenation of generated alkene from the carbenium ion or hydride transfer from the other alkane to the

50 carbenium ion. If the alkane produced from APAHs is not cracked but keeps the long chain length, the yield of

51 middle distillates such as light oil, kerosene, and >C20 alkanes for lubricating oil can be maximized. On the other

52 hand, the produced polycyclic aromatic hydrocarbons such as naphthalene, anthracene, phenanthrene, pyrene, etc.

53 can be converted by partial hydrogenation of the aromatic rings into tetralin derivatives, e.g., naphthalene into

54 tetralin [16-18]. Then, tetralin derivatives are converted into benzene derivatives through ring-opening [19,20]. In fact,

55 BTX production from PAHs has been recently reported [21-23]. Thus, this alternative process to the conventional

56 processes can maximize the amounts of long-chain alkanes and benzene derivatives with the minimum

57 consumption of hydrogen, compared to the hydrocracking process. We have previously reported the dealkylation as

58 a model reaction, in which only the C16 and 18 alkylnaphthalenes were fed as the reactant [6]. The next report

59 revealed the influence of coexisting substances in VGO as real heavy oil on the conversion of C16

60 alkylnaphthalene added as an index reactant [7]. However, the reactivity of original hydrocarbons in VGO has not

61 been apparent. It is essential for a commercialized process to comprehend the change of carbon balance in the

62 reaction.

63   In this study, dealkylation of APAHs in practical VGO is made solely to proceed over various solid acids

64 under hydrogen atmosphere. However, the solid acids are poisoned by basic nitrogen-containing compounds in the

65 original VGO. Before the dealkylation, the basic nitrogen-containing aromatic hydrocarbons were removed by

66 acidic ion-exchanged resins (containing a SO_3H group) [7]. The industrial utilization of this resin may be difficult due

67 to the expensiveness and the laborious regeneration, but we have recently found that the alternative to the resin was

68 inexpensive amorphous silica-alumina, which could be simply regenerated by heating [8]. Benzene was added for

69 increasing the fluidity. However, actual processes were operated in a flow of high-viscosity crude oil, and our

70 dealkylation process should be also applied at large scales without addition of benzene. The dealkylation activity

71 was compared among aluminosilicates: such as amorphous silica-alumina, zeolites, and a silica monolayer loaded

72 on alumina (SMA) as a candidate of catalyst. SMA can be synthesized by chemical vapor deposition (CVD) of Si

73 precursor on the surfaces of alumina and has been found to have catalytic activity for Brønsted acid-catalyzed

74 reactions [24,25]. SMA with 8–12 nm^{-2} of the Si concentration showed high activity and selectivity for dealkylation of

75 C16, 18 alkylnaphthalene into naphthalene and C16, 18 alkanes [6]. Therefore, SMA with 8 nm^{-2} of the Si

concentration were prepared for the dealkylation of APAHs in the practical VGO. Additionally, it was presumed that the textural properties of SMA affected the dealkylation activity in the practical VGO, which contained bulky hydrocarbons to prevent the diffusion of the reactants. In order to investigate the influence of pore size on dealkylation activity, SMA with different pore sizes from 6.2 to 33 nm were synthesized. In the reaction, a small amount of hydrogen is fed for hydrogenation of the alkenes, which are produced by the dealkylation and contained in the practical oil, because formation of coke from the alkenes deactivates the solid acid. The previous study mainly reported the reactivity of C16, 18 alkylnaphthalene, as a model reactant for indexing the dealkylation rate, in the coexistence of VGO components to quantitatively show the activity of SMA catalyst [7], and here the reactivity and selectivity of dealkylation of practical VGO components are evaluated with the aid of the two-dimensional GC (2D-GC) technique, in order to clarify changes in compositions of existing hydrocarbons in VGO. The high dealkylation activity and selectivity of long-chain alkanes of SMA, due to weak Brønsted acidity and large pore size, will be focused on.

2. Experimental

2.1. Catalyst preparation

Thin silica layers were prepared by means of a CVD (chemical vapor deposition) method [25] on the alumina materials JRC-ALO-6, -7, and -9, which had been supplied by Catalysis Society of Japan as reference catalysts, and a purchased sample from FUJIFILM Wako Pure Chemical Corp. The deposition was performed in a vacuum system using $Si(OCH_3)_4$ (tetramethoxysilane) as the precursor of silica. After evacuation of the support alumina at 673 K for 2 h, vapor of tetramethoxysilane was admitted contacting with alumina at 593 K, and the resultant increase of weight was monitored using a quartz spring balance. The supply of tetramethoxysilane vapor and evacuation were repeated to feed the precursor vapor and to remove the gaseous products continuously. The degree of vacuum was ca. 10^{-3} Torr (1 Torr = 133.3 Pa), and the vapor pressure of alkoxide was kept at ca. 2.5 Torr by chilling the reservoir with an ice bath. After a weight increase corresponding to SiO_2 with ca. 8 nm^{-2} of the Si concentration was observed, the sample was calcined in oxygen (200 Torr) at 673 K for 12 h. The amount of deposited Si was calculated from the weight increase while assuming that the formed material was SiO_2, and the

102   samples with ca. 8-9 Si atoms nm^{-2} were employed in the present study; hereafter, they are called SMA (silica

103   monolayer loaded on alumina). As a comparison, an amorphous silica-alumina catalyst industrially available,

104   N631-L (JGC Catalysts and Chemicals Ltd.), was tested for catalytic and analytical experiments, as well as the

105   following zeolites. An H-USY zeolite CBV720 with FAU structure (Si/Al$_2$= 29) was supplied by Zeolyst. In

106   addition, an NH$_4$-ZSM-5 zeolite HSZ820NAA with MFI structure (Si/Al$_2$= 22) was supplied by Tosoh Corp; it was

107   converted into H-ZSM-5 in the pretreatments for analytical and catalytic experiments.

108

109   2.2. Structural analysis

110   The nitrogen adsorption isotherm was measured at 77 K using BELSorp-max equipment

111   (Microtrac-BEL) after pretreatment at 573 K for 1 h. The surface area was calculated by the BET

112   (Brunauer-Emmett-Teller) equation [26], and the pore diameter distribution was analyzed from the desorption branch

113   using a BJH (Barrett-Joyner-Halenda) method [27].

114   The amount of chemisorbed benzoate anion was measured by a BAT (benzaldehyde-ammonia titration)

115   method [28]. About 40 mg of the sample was packed in a Pyrex tube (4 mm i.d.) and pretreated in an oxygen flow (27

116   μmol s^{-1}, atmospheric pressure) at 673 K for 1 h. Benzaldehyde (9.8 μmol) was injected into the sample bed at 573

117   K in a helium flow (27 μmol s^{-1}, atmospheric pressure), and the eluted aldehyde was monitored by a GC (GC-8A,

118   Shimadzu) with a silicone SE-30 packed column and an FID (flame ionization detector). The injection of the

119   aldehyde was repeated several times until the saturation of adsorption was observed, and then ammonia (0.41

120   mmol) was repeatedly supplied at 673 K. The formed benzonitrile was quantified by the GC, and the coverage was

121   calculated on the assumption that the benzoate anion was adsorbed only on the exposed alumina surface, not on the

122   silica-covered surface [25].

123   The ammonia IRMS (infrared / mass spectroscopy) -TPD (temperature-programmed desorption) method

124   was applied to measure the number and strength distribution of each of the Brønsted and Lewis acid sites [29]. A

125   self-supporting disc (1 cm diameter), molded from the sample by compression, was held by a set of metal rings to

126   fix in a cell of Microtrac-BEL IRMS-TPD analyzer and pretreated at 823 K in oxygen. The IR (infrared) spectra

127   were collected by an IR spectrometer (JASCO, FT/IR-4200) equipped with an MCT (mercury cadmium telluride

128   detector) while heating the sample in a helium flow (68 μmol s⁻¹, 6 kPa) at 2 K min⁻¹. Then ammonia was adsorbed

129   at 343 K, and the sample was again heated under the same conditions. The IR spectra and MS response (measured

130   by Pfeiffer Vacuum QMG220) were recorded. The ammonia TPD profile of each of the Brønsted and Lewis acid

131   sites was analyzed according to our previous study [30]. The number of acid sites was calculated from the peak

132   intensity of the TPD, and the distribution of enthalpy of ammonia desorption (so-called adsorption heat) was

133   analyzed by the curve fitting method [31].

134

135   2.3. Dealkylation of APAHs

136   The reactant for dealkylation of APAHs was prepared as follows. An isomer mixture of

137   hexadecylnaphthalene (HDN) with one alkyl branch, whose carbon number was 16, was purchased from Exxon

138   Mobil Corp. as a commercial sample Synesstic 5. VGO, yielded by vacuum distillation of a Middle East origin

139   crude oil (final boiling point at 1008 K, specific gravity 0.915 g cm⁻³, C: 85.11 wt%, H: 12.35 wt%, S: 2.35 wt%,

140   N: 0.06 wt%), was mixed with benzene and the above HDN. The composition of VGO:benzene:HDN was 1:1:0.11

141   in weight ratio. Here benzene was added for increasing the fluidity, in order to mix the resulting VGO with

142   adsorbent for the removal of basic compounds and to feed it with a pump for the reaction tests. HDN was added as

143   an index reactant for quantitative evaluation of catalytic activity for the dealkylation of APAHs. Then, for the

144   removal of basic compounds, a cation exchange resin (Amberlyst-15DRY, purchased from Organo) after

145   pretreatment at 353 K overnight was added into the VGO; 10 wt% of Amberlyst-15DRY based on the VGO was

146   used. The resulting mixture was stirred at room temperature for 1 h, and then the Amberlyst-15DRY was removed

147   by filtration. The above cation exchange resin treatment was repeatedly carried out (usually 2-3 times) until the pH

148   trend indicated the neutralization point as observed using an automatic neutralization titrator (916Ti-Touch,

149   Metrohm AG) [7,8].

150   The reaction was carried out by a fixed-bed continuous-flow method. The catalyst was packed in a

151   stainless steel tube (4 mm i.d.). The catalyst (210 mg) was pretreated in a flow of hydrogen (0.12 mol h⁻¹) under

152   atmospheric pressure at 773 K for 1 h. Then, the reactant was fed at 1.2 g h⁻¹ with a hydrogen flow (0.12 mol h⁻¹)

153   through the catalyst bed at 723 K. The total pressure in the tube was kept at 1 MPa using a back pressure valve

154 connected to the outlet. The formed material was trapped in a glass tube chilled with an ice bath. The products were

155 analyzed using a 2D-GC (Agilent 7890) with an FID and two capillary columns (0.25 μm thickness DB-5MS,

156 length 30 m, i.d. 0.250 mm, and 0.15 μm thickness DB-17HT, length 5 m, i.d. 0.250 mm). An internal standard

157 method was adopted with tetraethylene glycol dimethyl ether as the standard compound added after collecting the

158 products. The composition of the components based on the number of carbon atoms was calculated from the

159 relative intensities of GC peaks:

160
$$\text{composition} = \frac{\text{amount of carbon in each components in liquid (c} - \text{mol)}}{\text{amount of carbon in feedstock (c} - \text{mol)}} \times \text{fraction of recovered liquid}$$

161 HDN conversion was calculated as follows:

162
$$\text{conversion} = \frac{\text{amount of recovered HDN in liquid (c} - \text{mol)}}{\text{amount of feeded HDN (c} - \text{mol)}} \times \text{fraction of recovered liquid}$$

163 Light hydrocarbons were recovered by a gas pack and analyzed using GC equipment (GC-2014, Shimadzu) with an

164 FID and a capillary column (InertCap1, 5.0 μm thickness, 30 m in length, and internal diameter of 0.53 mm). The

165 composition averaged during 2-8 h of the time on stream was calculated:

166
$$\text{composition} = \frac{\text{amount of carbon in each components in gas (c} - \text{mol)}}{\text{amount of carbon in feedstock (c} - \text{mol)}} \times \text{fraction of recovered gas}$$

167 The structure and composition of residues adsorbed on the catalysts after the reaction were investigated

168 with elemental analysis and infrared (IR) spectroscopy. The catalysts were recovered after the reaction and dried at

169 room temperature under vacuum. An elemental analysis of the catalysts was carried out with a Vario EL cube

170 (Elementar Analytical). In the IR measurement, a self-supporting disc (1 cm diameter) was molded from a ground

171 mixture of the catalyst and potassium bromide (1:10 in weight ratio). It was set in a Microtrac BEL, IRMS-TPD

172 analyzer. After removal of water adsorbed on the catalyst under vacuum at 473 K for 0.5 h, the IR spectrum was

173 recorded under vacuum at 293 K.

174

175 **3. Results**

176 3.1. Physical properties and acidity profiles

177 **Table 1** shows physical properties of the silica monolayer deposited on alumina (SMA). The amount of

178 deposited material is here indicated by the surface concentration (Si atoms nm^{-2}). The coverage of surface by silica

179 was calculated by the BAT method. At 8.3 ± 0.4 nm^{-2}, the coverage of all the SMA samples exceeded 85%. It tells

180 us that a monolayer of silica with 1:1 Al-O-Si bonding was formed to cover almost completely the Al$_2$O$_3$ surface

181 [25,32]. BET surface areas of SMA before and after silica deposition are indicated in **Table S1** and **Table 1**,

182 respectively. The BET surface area of SMA (after the CVD) divided by the weight of alumina was not largely

183 different from the value before silica deposition, in all the cases, indicating that the surface area was unchanged by

184 the CVD. The mean pore diameter and mesopore volume of SMA before and after silica deposition are also shown

185 in **Table S1** and **Table 1**, respectively, and the pore size distribution in the mesopore region is shown in **Figure S1**.

186 The pore size and its distribution of SMA were generally close to those of the original Al$_2$O$_3$. The order in mode

187 value of pore size was SMA-1 (6.2 nm) < SMA-2 (9.2 nm) < SMA-3 (24 nm) < SMA-4 (33 nm), according to the

188 pore sizes of parent Al$_2$O$_3$. The mesopore volume increased with increasing the pore size. These textural profiles

189 indicate that the morphology of particles was retained, consistent with that a very thin layer of silica was formed on

190 alumina. The physical properties of amorphous silica-alumina (N631-L) and the zeolites (USY and ZSM-5) are

191 indicated in **Table 2**. The BET surfaces of amorphous silica-alumina and zeolites were higher than those of SMAs.

192 The mesopore size of N631-L was smaller than those of SMAs. On the other hand, most of the active sites on the

193 zeolites are estimated to exist in the micropores, and the sizes of micropore channels in USY and ZSM-5 were ca.

194 0.7 nm and 0.6 nm, respectively, far smaller than the pores of SMAs and N631-L. The mesopore volume of N631-L

195 was similar to SMA-1, while the zeolites possessed small volumes of mesopores, mainly located between the

196 crystal grains.

197   The ammonia IRMS-TPD determined the acidic properties [30]. **Figures S2** and **S3** show the IR spectra

198 obtained on the catalysts during the TPD experiments. A sharp band at ca. 1450 cm^{-1} was assigned to bending (v_4)

199 vibration of NH$_4^+$ adsorbed on Brønsted acid sites (NH$_4^+$ (BAS)). A small peak at 1250-1330 cm^{-1} was assigned to

200 bending (δ_s) vibration of ammonia adsorbed on Lewis acid sites (ammonia (LAS)). **Figure S4** shows TPD profiles

201 of ammonia desorbed from the acid sites. MS-TPD indicates the profile of ammonia desorption evaluated with

202 mass spectroscopy. The TPD profiles were calculated from the IR-TPD of ca. 1450 cm^{-1}-band (v_4, NH$_4^+$ (BAS))

203 and 1250-1330 cm^{-1}-band (δ_s, ammonia (LAS)), respectively [30]. **Table 3** shows the amount and strength of BAS.

204 Mode value in enthalpy (ΔH) of ammonia desorption from the BAS on catalysts is indicated as an index of

205   Brønsted acid strength (distribution of ΔH is shown in **Figure S5**) [33]. No difference was found in the strength of

206   BAS on the SMAs as shown by ΔH. The amount of BAS on SMA distributed in 0.06-0.11 mol kg^{-1} (0.25-0.36 nm^{-2}

207   on the surface area basis). The amorphous silica-alumina (N631-L) had more than 1.5 times the BAS of SMAs, and

208   the acid strength on N631-L was higher than those on SMAs. The amount of BAS on the zeolites (USY and

209   ZSM-5) was more than SMAs and N631-L, and BAS on the zeolites was much stronger as estimated from ΔH.

210   Especially, ZSM-5 possessed stronger BAS in a high density.

211

212   3.2. Dealkylation of alkyl aromatic hydrocarbons

213   SMA-3 exhibited high activity and selectivity in the model reaction of HDN as previously reported [6], and

214   was thus compared with various aluminosilicates as solid acids in this section. Hexadecylnaphthalene (HDN) was

215   added to VGO as an index reactant, and the reactivity was assessed by the conversion of this compound. **Figure 1**

216   shows the time courses of HDN conversion on various solid acids. At 2 h of the time on stream, all the catalysts

217   showed almost equivalent conversion values. Decline in the reaction rate was in the order of N631-L < SMA-3 <

218   USY << ZSM-5. Here it is noted that the previous studies have revealed the highest activity of SMA for the

219   conversion of HDN at 673 K among the solid acids which were tested also in the present study [6,7]. The present

220   experiments were performed at 723 K for evaluation of the catalytic performances under practical conditions, and

221   therefore the apparent order of conversion was somewhat different.

222   This study quantified not only the HDN conversion but also changes in the hydrocarbon compositions by

223   the reaction over aromatics and aliphatics. The compositions of the products in the reactions on the catalysts are

224   shown in **Tables S2-S5**. The time courses of composition of APAHs in outlet products are shown in **Figure 2**. The

225   original (fed) VGO contained 32 c-mol% of APAHs including HDN. SMA-3 reduced the APAHs content down to 8

226   c-mol% constantly at 2-8 h of the time on stream, indicating that dealkylation of APAHs proceeded, and the

227   catalytic activity was stably maintained. On N631-L and USY, the recovery of APAHs was high at the initial stage

228   of the flow reaction, indicating the low activity, and the recovery decreased with the time on stream. On ZSM-5,

229   more than half of the APAHs was eluted at the initial stage (2-4 h of the time on stream), showing the low activity,

230   and the recovery gradually increased with the time on stream, indicating quick deactivation of the catalyst. These

231   results indicate that the dealkylation activity of SMA-3 was higher than those of the amorphous silica-alumina and

232   zeolites. However, 8 c-mol% of the APAHs was unreacted even on SMA-3. **Figure S6** shows composition of alkyl

233   groups in alkyl bicyclic and tricyclic aromatics in the products over SMA-3 during 2-8 h of the time on stream.

234   Most of the side chains before the reactions possessed >5 carbon atoms in an alkyl group. The dealkylation on

235   SMA-3 reduced the carbon number down to <5. It means that the APAHs with long-chain alkyl groups were mainly

236   dealkylated, while the methyl and ethyl groups attached to the polyaromatic rings showed lower reactivity on

237   SMA-3.

238   **Figure 3** shows the time courses of composition of alkylbenzenes (alkyl monocyclic aromatics) in outlet

239   products. The original VGO contained 9 c-mol% of alkylbenzenes. SMA-3 reduced alkylbenzenes in a small

240   amount down to 7 c-mol%, while the amorphous silica-alumina and zeolites obviously increased the alkylbenzenes.

241   More than half of outlet liquid and gas eluted in the reaction on ZSM-5 were alkylbenzenes in the initial time

242   period, but the yield decreased with the time on stream. Composition of the side chains in alkylbenzenes in the

243   products on SMA-3 is displayed in **Figure S7**. Most of the alkylbenzenes in the products possessed long-chain

244   alkyl groups, meaning that the alkyl monoaromatics were inactive regardless of the long chain length on SMA-3. It

245   was in contrast to the observations in the case of APAHs as stated above; the chain length of the alkyl group

246   affected the reactivity in the case of APAHs. It is concluded that SMA-3 was active for the dealkylation of APAHs

247   with long-chain alkyl groups but inactive for the reactions of alkyl monoaromatics and APAHs with short-chain

248   alkyl groups.

249   **Figure 4** shows the time courses of composition of the alkanes in the products. The original VGO

250   contained 56 c-mol% of long-chain aliphatics (>C20); here it is noted that the original VGO contained alkanes and

251   alkenes, whereas the outlet products contained mainly alkanes due to the reaction in pressurized hydrogen. ZSM-5

252   markedly decreased the >C20 alkanes, suggesting the progress of cracking of alkane. USY and N631-L also

253   showed decreases of >C20 alkanes composition. SMA-3 also reduced the >C20 alkanes, but the extent was less

254   than the amorphous silica-alumina and zeolites to keep the composition at 44 c-mol% during 5-8 h (**Figure 4 (A)**).

255   On the other hand, the original VGO contained only 4 c-mol% of C10-20 alkanes and no <C5 alkanes. Formation

256   of <C20 alkanes presumably due to the dealkylation of aromatics was observed as shown in **Figure 4 (B)** and **(C)**.

SMA-3 and N631-L produced more C10-20 alkanes than the zeolites, while C5-9 alkanes were produced in the following order: N631-L > USY ≈ SMA-3 > ZSM-5. **Figure 5** shows the composition of light hydrocarbons during 2-8 h of the time on stream. The yield of light hydrocarbons was in the following order: SMA-3 < N631-L < USY < ZSM-5. The composition of C4-6 in the light hydrocarbons over SMA-3, N631-L, and USY was >60%, while ZSM-5 produced excessive amounts of C1-3 alkanes. Here it is emphasized that ZSM-5 did not produce C5-20 alkanes but C3-4 alkanes in large quantities.

A gradual decline in the dealkylation activity was observed as displayed in **Figures 1 and 2**. The substances adsorbed on the catalysts during the reactions were analyzed by elemental analysis (**Table 4**) and IR measurements (**Figure 6**). The amount of deposited carbon was in the following order: SMA-3 < ZSM-5 < N631-L < USY. Hydrogen was also detected, whereas trace amounts of nitrogen and sulfur were observed. The molar ratio of hydrogen to carbon (H/C) on USY was <1, indicating that the adsorbed hydrocarbons were polyaromatics (PAHs). H/C on SMA-3 and N631-L was close to 2, and therefore alkanes or long-chain alkylaromatics were presumed to be formed. ZSM-5 showed higher H/C than the other catalysts. IR spectra of the catalysts after the reaction indicated the existence of aromatics and alkanes. An absorption band at 1600 cm^{-1} was assigned to C=C stretching vibration in aromatics, and the absorbance was in the following order: USY > ZSM-5 > N631-L > SMA-3. A pair of absorption bands at 2850 and 2900 cm^{-1} was assigned to C-H stretching vibration in alkanes and/or alkyl groups (in alkylaromatics) and observed in all the spectra. The deposited substances on USY are thus revealed to have been predominantly PAHs, while the substances on N631-L and SMA-3 were alkanes and small amounts of alkylaromatics. The adsorbed substances on ZSM-5 were mostly alkyl aromatics; too high a H/C ratio suggests the presence of water condensed in the micropores.

3.3. Influence of textural property of SMA on activity and selectivity in the dealkylation

As stated in the last section, SMA efficiently catalyzed the dealkylation of APAHs into PAHs and long-chain alkanes. As previously reported, the activity of SMA for the dealkylation of a model substance was created by the deposition of silica monolayer with Brønsted acidity, and the activity showed the maximum on the catalyst where the coverage by the monolayer was the maximum, presumably due to high density of Brønsted acid

283   sites [6]. Therefore, the importance of Brønsted acidity is undoubtable for the activity of SMA in the dealkylation of

284   APAHs. However, the low selectivity of amorphous silica-alumina (mesoporous) and zeolites (microporous) as

285   shown in the last section suggests the influence of the porous nature on this reaction. It is presumed that the textural

286   properties of the catalyst affected the activity for the dealkylation of APAHs in the practical VGO, which contained

287   bulk hydrocarbon molecules, and their diffusion was prevented to some extent. Accordingly, the pore size of SMA

288   was varied, and its influence was investigated. SMA-1 to -4 were prepared by the deposition of silica monolayer on

289   γ-alumina samples with different pore sizes from 6 to 33 nm; the resultant pore sizes of SMA were similar to the

290   pore sizes of the support alumina samples (**Table 1** and **Table S1**). The number of Brønsted acid sites normalized

291   by catalyst weight or surface area was not largely different (within 0.06-0.11 mol kg^{-1} or 0.25-0.36 nm^{-2}), as well,

292   Brønsted acid strength (ΔH) was similar as shown in **Table 3**. The similar acidic properties suggest a principally

293   same chemical nature of SMA surface due to equivalent microstructure. It is concluded that the SMA-1 to -4 had

294   similar microstructures and Brønsted acidic properties, but the porous nature at 1-10 nm dimensions was different.

295   The activities of SMA in the dealkylation are shown in **Figures S8-S11**. The composition of components

296   in the reactions over all the catalysts displayed analogous changes over the time on stream, and was steady during

297   5-8 h. **Figure 7** shows the average composition of components during 5-8 h in the dealkylation over SMAs. Both

298   the APAHs and PAHs were retrieved in the same amount over all the SMAs. This tells us that the dealkylation

299   activities of all the SMA catalysts were comparable. The amount of alkylbenzenes after the reaction was almost the

300   same as the original amount in VGO. Long-chain alkanes (>C20) relatively decreased over SMA-1 and -2,

301   compared with SMA-3 and -4, while the composition of light hydrocarbons was in the following order: SMA-2 >

302   -1 > -3 > -4. There were no differences in yield of C10-20 and C5-9 alkanes among all the catalysts. A part of

303   long-chain alkanes was thus observed to be cracked into C5-9 alkanes, but deep cracking into C1-6 alkanes

304   proceeded only on the SMA with relatively small mesopore size.

305

306   **4. Discussion**

307   The assumed novel upgrading process consists of the dealkylation of APAHs in the feed mixture and the

308   separation of aromatics (polar) and alkanes (non-polar) based on the large difference in polarity. The alkyl aromatic

12

molecules possessing long alkyl chains with high compatibility should hinder the polar separation. Therefore, they need to be completely dealkylated. Alkanes are usually contained in the feed oil and produced by the dealkylation. Among the alkanes, the C5-10, C10-20, and larger alkanes are utilized as gasoline, diesel fuel, and lubricating oil, respectively, while the short chain (<C4) alkanes, i.e., off gas, are useless. The long-chain alkanes can be converted into alkanes suitable for gasoline and diesel fuel, and monocyclic aromatics by the conventional FCC if necessary, while the off-gas components are difficult to convert into valued compounds. Therefore, in the dealkylation step, the chain length of alkanes and alkyl groups in the alkyl aromatics should be kept; therefore, cracking of alkanes, a side reaction, needs to be restricted, and high yield of long-chain alkanes is desirable. For the above reactions, this research target is to find the catalyst which shows high conversion of APAHs and selectivity of long-chain alkanes in the dealkylation. High HDN conversion and decrease of recovered APAHs show high catalytic activity for the desired reaction (dealkylation of APAH), while production of large amounts of recovered long-chain alkanes (C10-20 for diesel fuel and >C20 for lubricating oil) and small amounts of recovered C5-9 alkanes and light hydrocarbons shows the high selectivity for the desired reaction.

HDN conversion was in the order ZSM-5 < USY < SMA-3 < N631-L, while amounts of recovered APAHs were SMA-3 < N631-L ≈ USY < ZSM-5. HDN conversion on SMAs gradually decreased in **Figures 1** and **S8**. The catalysts were deactivated by the adsorption of long-chain alkanes, but the deactivated catalysts can be regenerated by calcination at 773 K in oxygen flow [7]. No difference among the SMAs was found in HDN conversion and amounts of recovered APAHs. In addition, the order of amounts of recovered alkylbenzenes was SMA-3 < N631-L < USY << ZSM-5; the amount of alkylbenzenes increased from the original VGO on catalysts other than SMAs, indicating the formation of alkylbenzenes. Amount of total recovered long-chain alkanes (C10-20 and >C20) was in the following order: ZSM-5 < USY < N631-L < SMA-3. In light alkanes, C5-9 alkanes were produced in the order ZSM-5 < SMA-3 ≈ USY < N631-L, while yield of light hydrocarbons was SMA-3 < N631-L < USY < ZSM-5. Total images of the reactions on the catalysts are shown in **Figure S12**. The bracketed values were calculated on the basis of **Tables S2-5** and averaged over 5-8 h in the reactions. The width of the arrows in the images indicates the amount of changes of hydrocarbons. SMA-3 reduced more APAHs and HDN (a total of 7.6 wt% from 30.6 c-mol%) and showed more yield of >C20 alkanes (45.7 c-mol%), indicating that SMA-3 exhibited

13

335 high dealkylation activity and high selectivity of long-chain alkanes. N631-L and USY showed higher yield of

336 short-chain alkanes (C5-9 alkanes and light hydrocarbons) than SMA-3, due to the cracking of alkanes. ZSM-5

337 showed higher yield of APAHs and HDN, but less yield of >C20 and C10-20 alkanes (a total of 16.8 c-mol%) than

338 the other catalysts. In comparison by SMA, >C20 alkanes were less over SMA-1 and -2 than SMA-3 and -4, while

339 yield of light hydrocarbons was in the following order: SMA-4 < -3 < -1 < -2. However, there were no differences

340 in yield of C10-20 and C5-9 alkanes among the SMAs.

341   The pore size was found to be ZSM-5 < USY < N631-L < SMAs, while the Brønsted acid strength was

342 SMAs < N631-L < USY < ZSM-5. Among SMAs, mode value of pore size was in the order SMA-1 < -2 < -3 < -4,

343 whereas all the catalysts possessed a similar amount and strength of Brønsted acid sites.

344   The previous studies revealed high activity of SMAs in the dealkylation of model APAH reactant [6,7]. This

345 study confirms the higher conversion of APAHs in the practical oil and selectivity of long-chain alkanes on SMAs

346 than amorphous silica-alumina and zeolites. The high conversion on SMAs is related to the large pore size. It is

347 supposed that the bulky reactant molecules can penetrate into the large pore of SMAs and then be dealkylated into

348 alkanes and PAHs. On the other hand, the cracking of alkane is more difficult, from the viewpoint of acid-catalysis

349 chemistry, than dealkylation of alkyl aromatics, because it needs a strong Brønsted acid site as follows. The

350 dealkylation of APAHs proceeds through attack of H^+ on the aromatic ring and then formation of the carbenium ion

351 (arenium ion) for relatively stable intermediates of σ-complex, and finally produces PAHs and alkenes

352 (subsequently hydrogenated into alkanes). The aromatic rings are subject to nucleophilic attack, and therefore the

353 dealkylation proceeds on even weak Brønsted acid sites. On the other hand, cracking of alkane proceeds through

354 formation of an alkanium ion by attack of H^+ and then the protolytic cracking into a carbenium ion and an alkane

355 (or a dihydrogen). Alkanium ion is an unstable intermediate, and therefore the cracking proceeds on only strong

356 Brønsted acid sites. Weak Brønsted acid sites on SMAs cannot catalyze the cracking of both alkanes and alkyl

357 groups in APAHs. According to these explanations, the high selectivity (low activity for alkane cracking) of SMA is

358 considered to be due to the moderate Brønsted acid strength, and alkyl groups in the reactants and the produced

359 alkanes were difficult to crack into lighter alkanes. Thus, the large pore size and moderate Brønsted acid strength

360 are concluded to generate the high activity and selectivity of SMA for the dealkylation of APAHs.

361   A difference between APAHs and alkylbenzenes was observed in the reaction over SMAs; the SMA was

362   inactive for the dealkylation of alkyl monocyclic aromatics but active for the dealkylation of APAHs. The arenium

363   ion formed from APAHs holds a higher variety of resonance structures than that formed from alkylbenzenes. Due to

364   the higher stability of the intermediate, the APAHs should be more reactive than the alkylbenzenes. As a result, the

365   SMA catalyzed the conversion of APAHs but kept the alkylbenzene, which is directly useful for chemical resources,

366   adding an advantage of the presently proposed process using SMA.

367   A part of APAHs remained on even SMAs, but most of them consisted of short (C1-4) alkyl groups.

368   Binding energy between alkyl groups and aromatic rings is in the following order: propyl < ethyl << methyl [34]. In

369   addition, the carbenium ion formed by the dealkylation is stable in the following order: tertiary carbon > secondary

370   carbon > primary carbon > methylium. From the above principles, the removal of methyl and ethyl groups from the

371   aromatic ring is estimated to be difficult compared to the >C3 alkyl groups. It is therefore reasonable to conclude

372   that methyl and ethyl groups, in some cases multiple ones in a molecule, were unreacted on SMA and detected as

373   the APAHs with C1-4 alkyl groups. The purpose of dealkylation is to separate the aromatic rings from alkanes

374   which are useful as fuel and/or the feeds of further treatment. The long-chain alkanes are useful as fuels and/or

375   feeds, but C1-4 alkanes are not, and therefore the observed inactivity of C1-4 alkyl groups does not reduce the

376   advantages of SMA for the dealkylation of APAHs.

377   N631-L and USY formed more APAHs in the initial time period than during 6-8 h. The dealkylation of

378   APAHs and the cracking of alkanes probably proceeded, and then polymerization to APAHs deactivated a part of

379   the acid sites such as strong Brønsted acid sites. However, only the dealkylation proceeded with time. On the other

380   hand, ZSM-5 substantially catalyzed cracking of long-chain alkanes and produced lighter alkanes along with

381   formation of alkylbenzenes by swift cyclization of alkenes. N631-L exhibited higher activity in the dealkylation

382   than SMAs (**Figures 1 and 2**) but formed APAHs by the cracking and polymerization of alkanes in the initial time

383   period (**Figure 2**). Therefore, the order of conversion in **Figure 1** was different from the order of composition of

384   APAHs in **Figure 2**. However, carbon deposition on ZSM-5 also deactivated the acid sites, and the reaction rate in

385   the dealkylation of APAHs decreased with the time on stream. From the above results, APAHs on N631-L, USY,

386   and ZSM-5 were recovered more than SMAs, and the cracking of long-chain alkanes proceeded.

387   SMAs exhibited the same dealkylation activity, but a difference of alkane selectivity was observed. The

388   selectivity of long-chain alkanes (>C20) on SMA-1 and -2 was less than that on SMA-3 and -4, while the

389   composition of light hydrocarbons was in the following order: SMA-2 > -1 > -3 > -4. It was speculated that

390   long-chain alkanes were prone to contact with acid sites due to high surface area on SMA-1 and -2, otherwise due

391   to capillary condensation in the smaller mesopores in SMA-1 and -2 than that in SMA-3 and -4. Therefore, SMA-3

392   and -4, which had weak Brønsted acid sites and large pores, exhibited higher dealkylation activity and selectivity of

393   long-chain alkanes than the other solid acids including SMA-1 and -2. However, the pore size did not determinately

394   influence the dealkylation activity. Therefore, production of SMA catalysts for dealkylation should be

395   commercially practicable.

396

397   **5. Conclusions**

398   A silica-monolayer loaded on alumina (SMA) with weak Brønsted acid sites and large pore size catalyzed

399   dealkylation of APAHs in a practical heavy oil such as VGO, and exhibited higher activity and selectivity of

400   long-chain alkanes than amorphous silica-alumina (N631-L) and the zeolites (USY and ZSM-5). High activity on

401   SMAs was proposed to be due to larger pore size in which APAHs could sufficiently diffuse. Some APAHs were

402   retrieved, but combined with multiple methyl or ethyl groups. The residual should not affect separation of alkanes

403   and PAHs by solvent extraction. On the other hand, the produced alkanes and alkyl groups in the reactants were not

404   cracked on weak Brønsted acid sites in SMAs. The retrieved >C20 and C10-20 alkanes can be utilized as

405   lubricating oil and light oil or kerosene, respectively. On the hand, C5-9 alkanes and light hydrocarbons were

406   hardly formed. Analyses of SMA after the reaction found adsorbed alkanes, which did not lead to drastic

407   deactivation. Additionally, pore size of SMA increased with limiting cracking of long-chain alkanes, and the

408   catalysts with larger pores exhibited higher selectivity of long-chain alkanes. The dealkylation produced long-chain

409   alkanes and PAHs, which can be converted to benzene derivatives through further treatment. Catalytic reforming of

410   long-chain alkanes may form benzene, toluene, and xylenes, whereas PAHs are converted into tetralin derivatives

411   through partial hydrogenation, and further ring-opening of the naphthene in tetralin derivatives produces benzene

412   and its derivatives. These processes for production of the aromatics will be studied as future work.

413

Conflicts of interest

There are no conflicts to declare.

416

Acknowledgements

421

References

1 J. Chang, N. Tsubaki and K. Fujimoto, *Fuel*, 2001, **80**, 1639–1643.

2 R. Yoshida, M. Miyazawa, H. Ishiguro, S. Itoh, K. Haraguchi, H. Nagaishi, H. Narita, T. Yoshida, Y. Maekawa and Y. Mitarai, *Fuel Process. Technol.*, 1997, **51**, 195–203.

3 R. Yoshida, M. Miyazawa, T. Yoshida, H. Narita and Y. Maekawa, *Fuel*, 1996, **75**, 99–102.

4 R. Yoshida, T. Yoshida, H. Narita and Y. Maekawa, *Fuel*, 1986, **65**, 425–428.

5 Organization of the Petroleum Exporting Countries, World Oil Outlook 2019.

6 N. Katada, Y. Kawaguchi, K. Takeda, T. Matsuoka, N. Uozumi, K. Kanai, S. Fujiwara, K. Kinugasa, K. Nakamura, S. Suganuma and M. Nanjo, *Appl. Catal. A Gen.*, 2017, **530**, 93–101.

7 K. Kinugasa, F. Nakano, S. Nagano, S. Suganuma, E. Tsuji and N. Katada, *J. Japan Pet. Inst.*, 2018, **61**, 294–301.

8 S. Suganuma, K. Arita, F. Nakano, E. Tsuji and N. Katada, *Fuel*, 2020, **266**, 117055.

9 K. Nakajima, S. Suganuma, E. Tsuji and N. Katada, *React. Chem. Eng.*, **5**, 1272–1280.

10 S. Suganuma and N. Katada, *Fuel Process. Technol.*, 2020, **208**, 106518.

11 S. W. Ferris, E. R. Birkhimer and L. M. Henderson, *Ind. Eng. Chem.*, 1931, **23**, 753–761.

12 A. De Lucas, L. Rodriguez, P. Sanchez and A. Carnicer, *Sep. Sci. Technol.*, 1993, **28**, 2465–2477.

13 B. Coto, R. van Grieken, J. L. Peña and J. J. Espada, *Chem. Eng. Sci.*, 2006, **61**, 8028–8039.

14 B. W. Wojciechowski, *Catal. Rev.*, 1982, **24**, 1–65.

15 A. M. Youssef, A. I. Ahmed and S. E. Samra, *Mater. Lett.*, 1990, **10**, 175–180.

16 M. Du, Z. Qin, H. Ge, X. Li, Z. Lü and J. Wang, *Fuel Process. Technol.*, 2010, **91**, 1655–1661.

17 A. Stanislaus and H. C. Barry, *Catal. Rev.*, 1994, **36**, 75–123.

18 Y. Choi, J. Lee, J. Shin, S. Lee, D. Kim and J. K. Lee, *Appl. Catal. A Gen.*, 2015, **492**, 140–150.

19 A. Corma, V. González-Alfaro and A. V. Orchillés, *J. Catal.*, 2001, **200**, 34–44.

20 M. Santikunaporn, J. E. Herrera, S. Jongpatiwut, D. E. Resasco, W. E. Alvarez and E. L. Sughrue, *J. Catal.*, 2004,

228, 100–113.

21 J. Shin, Y. Oh, Y. Choi, J. Lee and J. K. Lee, *Appl. Catal. A Gen.*, 2017, **547**, 12–21.

22 Y. Oh, J. Shin, H. Noh, C. Kim, Y. S. Kim, Y. K. Lee and J. K. Lee, *Appl. Catal. A Gen.*, 2019, **577**, 86–98.

23 Y. Oh, H. Noh, H. Park, H. Han, T. B. Nguyen and J. K. Lee, *Catal. Today*, 2020, **352**, 329–336.

24 M. Niwa, T. Hibino, H. Murata, N. Katada and Y. Murakami, *J. Chem. Soc. Chem. Commun.*, 1989, 289–290.

25 M. Niwa, N. Katada and Y. Murakami, *J. Phys. Chem.*, 1990, **94**, 6441–6445.

26 S. Brunauer, P. H. Emmett and E. Teller, *J. Am. Chem. Soc.*, 1938, **60**, 309–319.

27 E. P. Barrett, L. G. Joyner and P. P. Halenda, *J. Am. Chem. Soc.*, 1951, **73**, 373–380.

28 M. Niwa, S. Inagaki and Y. Murakami, *J. Phys. Chem.*, 1985, **89**, 3869–3872.

29 M. Niwa, K. Suzuki, N. Katada, T. Kanougi and T. Atoguchi, *J. Phys. Chem. B*, 2005, **109**, 18749–18757.

30 S. Suganuma, Y. Murakami, J. Ohyama, T. Torikai, K. Okumura and N. Katada, *Catal. Letters*, 2015, **145**, 1904–1912.

31 N. Katada, T. Tsubaki and M. Niwa, *Appl. Catal. A Gen.*, 2008, **340**, 76–86.

32 N. Katada, T. Fujii, K. Iwata, Y. Hibino and M. Niwa, *J. Catal.*, 1999, **186**, 478–480.

33 M. Niwa and N. Katada, *Chem. Rec.*, 2013, 13, 432–455.

34 M. Szwarc, *Chem. Rev.*, 1950, **47**, 75–173.

423

424   Table 1   Physical properties of the silica-monolayer deposited on alumina

Catalyst	Al$_2$O$_3$	Amount of SiO$_2$ [1] / wt%	Deposited Si atoms / nm^{-2}	Coverage / %	Surface area [2] / m^2 g^{-1}	Pore size [3] / nm	Mesopore volume [4] / cm^3 g^{-1}
SMA-1	Purchased sample [5]	14.1	8.5	86	184 [6] (214 [7])	6.2	0.36 [6] (0.42 [7])
SMA-2	ALO-9	14.2	8.1	90	182 [6] (212 [7])	9.2	0.58 [6] (0.68 [7])
SMA-3	ALO-6	13.3	7.9	91	169 [6] (195 [7])	24	0.83 [6] (0.96 [7])
SMA-4	ALO-7	13.1	8.7	95	147 [6] (169 [7])	33	0.95 [6] (1.09 [7])

425   [1] Normalization by catalyst weight, [2] calculated by BET equation, [3] mode value of pore size calculated by BJH

426   method, [4] calculated by BJH method, [5] sample purchased from FUJIFILM Wako Pure Chemical Corp., [6]

427   normalized by catalyst weight, [7] divided by the weight of alumina as a support.

428

429   Table 2 Physical properties of amorphous silica-alumina and zeolites

Catalyst	Surface area [*1] / m^2 g^{-1}	Pore size / nm	Micropore volume [*2] / cm^3 g^{-1}	Mesopore volume [*3] / cm^3 g^{-1}
N631-L	483	3.7 [*4]	<0.01	0.51
USY	756	0.74 × 0.74 [*5]	0.30	0.24
ZSM-5	308	0.53 × 0.56, 0.55 × 0.51 [*5]	0.13	0.12

430   [*1] Calculated by BET equation, [*2] calculated using *t*-plot method, [*3] calculated by BJH method, [*4] mode value of

431   pore size calculated by BJH method, [*5] estimated by crystal structures of zeolite.

432

433 Table 3 Acidic properties of solid acids

Catalyst	Brønsted acid amount / mol kg^{-1} (site nm^{-2}) [*1]	ΔH [*2] / kJ mol^{-1}
SMA-1	0.11 (0.36)	116
SMA-2	0.08 (0.26)	116
SMA-3	0.10 (0.36)	116
SMA-4	0.06 (0.25)	116
N631-L	0.17 (0.21)	122
USY	0.34 (0.27)	136
ZSM-5	1.14 (2.23)	148

434 [*1] Number of Brønsted acid sites normalized by BET surface area, [*2] mode value in enthalpy of ammonia

435 desorption from Brønsted acid sites.

436

437   Table 4   Elemental analysis of adsorbed substances on the catalysts after the dealkylation of APAHs in fed VGO

438   after 8 h time-on-stream at 723 K.

	wt%				Molar ratio
	C	H	N	S	H/C
SMA-3	5.43	0.80	Trace	Trace	1.77
N631-L	13.85	5.10	Trace	Trace	1.82
USY	22.09	1.56	Trace	Trace	0.85
ZSM-5	6.84	1.54	Trace	Trace	2.70

439

440

Figure Captions

Figure 1   Time courses of HDN (hexadecylnaphthalene) conversion on SMA-3 (●), N631-L (■), USY (◊), and ZSM-5 (△) in the dealkylation of APAHs in fed VGO at 723 K and LHSV = 5.7 g_{VGO} g_{cat}^{-1} h^{-1}.

Figure 2   Time courses of composition of APAHs in products on SMA-3 (●), N631-L (■), USY (◊), and ZSM-5 (△) in the dealkylation of APAHs in fed VGO at 723 K and LHSV = 5.7 g_{VGO} g_{cat}^{-1} h^{-1}. Double circle means the amount of APAHs in the original (fed) VGO.

Figure 3   Time courses of composition of alkylbenzenes in products on SMA-3 (●), N631-L (■), USY (◊), and ZSM-5 (△) in the dealkylation of APAHs in fed VGO at 723 K and LHSV = 5.7 g_{VGO} g_{cat}^{-1} h^{-1}.   Double circle means the amount of alkylbenzenes in the original (fed) VGO.

Figure 4   Time courses of composition of alkanes ((A): >C20, (B): C10-20, and (C): C5-9) in products on SMA-3 (●), N631-L (■), USY (◊), and ZSM-5 (△) in the dealkylation of APAHs in fed VGO at 723 K and LHSV = 5.7 g_{VGO} g_{cat}^{-1} h^{-1}. Double circle means the amounts of alkanes in the original (fed) VGO.

Figure 5   Composition of light hydrocarbons averaged during 2-8 h in the dealkylation of APAHs in fed VGO at 723 K and LHSV = 5.7 g_{VGO} g_{cat}^{-1} h^{-1}.

Figure 6   IR spectra of various solid acids after the dealkylation of APAHs in fed VGO after 8 h time on stream at 723 K. Red line: SMA-3, blue line: N631-L, green line: USY, and purple line: ZSM-5.

Figure 7   Compositions of outlet compounds averaged during 5-8 h on SMAs in the dealkylation of APAHs in fed VGO at 723 K and LHSV = 5.7 g_{VGO} g_{cat}^{-1} h^{-1}. The compositions in the original (fed) VGO are shown in a leftmost bar.
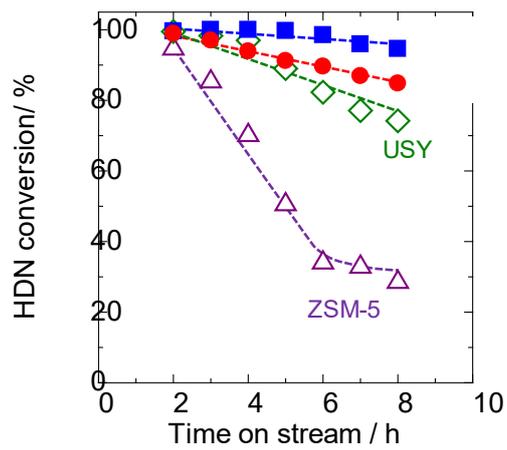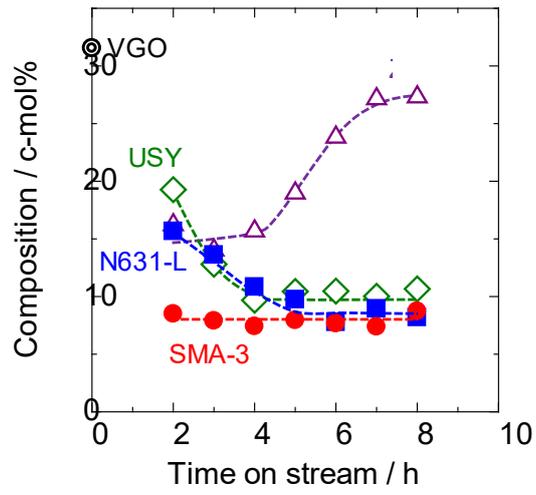
Figure 1

464

465

466

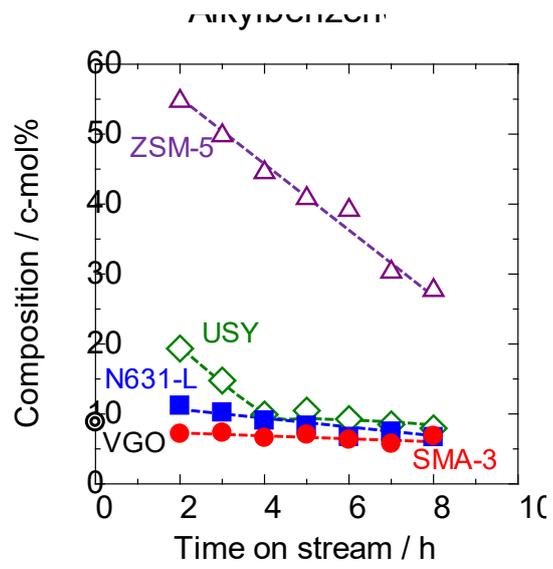## Alkyl polyaromatic hydrocarbons

Figure 2

467

468

469

470

Figure 3

474

475

476

Figure 4

477

478
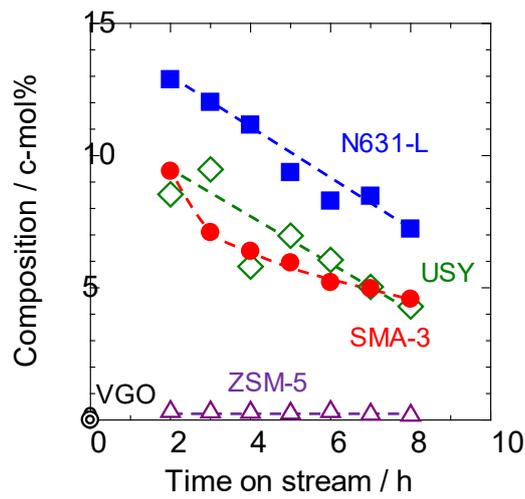
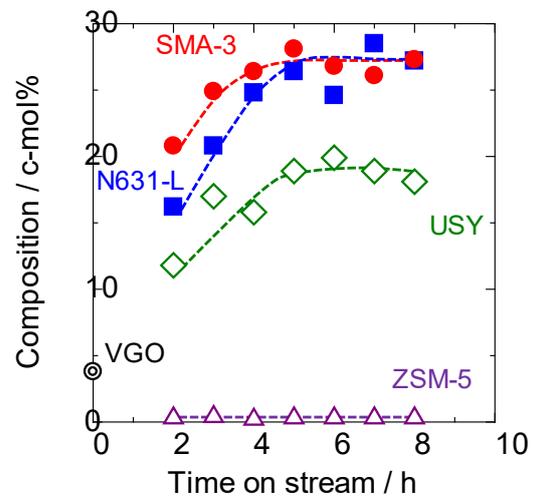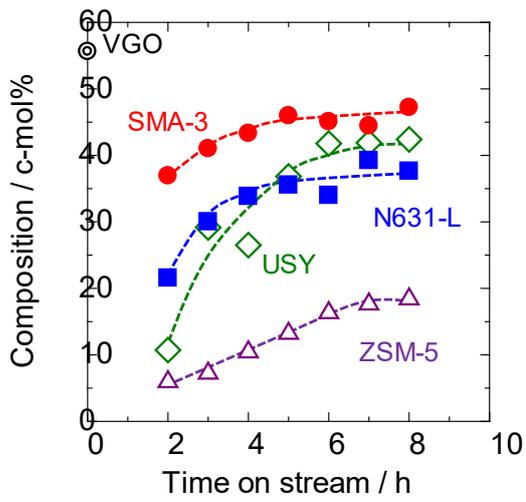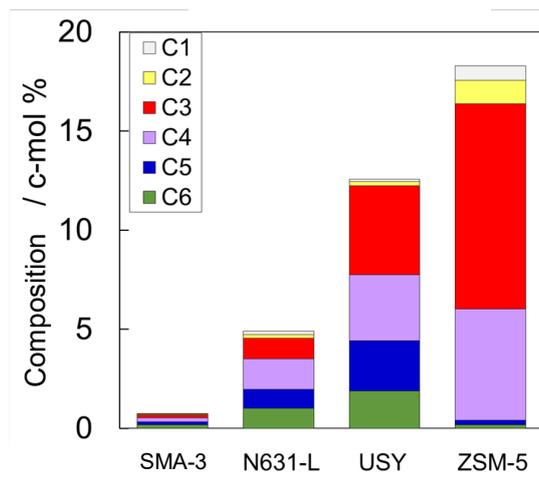|	SMA-3	N631-L	USY	ZSM-5
C1-3 (%)	26	28	37	66
C4-6 (%)	74	72	63	34

479

480 Figure 5

481

482

483

484   Figure 6

485

486

Figure 7

487

488

489